

Bandwidth enhancement of circular structure microstrip antenna based on inverted C-shaped ground configuration

Siswo Wardoyo*, Jaka Permana, Toto Supriyanto, Muh Wildan, Febrizal, Syah Alam, and Teguh Firmansyah

Abstract—Designing microstrip antennas with wide bandwidth and low-frequency capabilities presents several challenges. These difficulties mainly arise due to the relatively small size of the microstrip in comparison to the operating frequency. Therefore, achieving a combination of enhanced bandwidth and lower-frequency cut-off becomes crucial to support a broad frequency range of communication technologies. This paper presents a method for enhancing the bandwidth of a circular microstrip antenna based on an inverted C-shaped ground configuration. The proposed method successfully creates an antenna with extended bandwidth while lowering the operating frequency. The antenna was simulated and then fabricated using an RO5880 duroid substrate with a relative permittivity of 2.2, a thickness of 1.575 mm, and a loss tangent of 0.0009. The simulation and measurement results demonstrate that the antenna can operate effectively within a wide frequency range of 3.5 GHz to 18 GHz. Additionally, utilizing this method enables the antenna to function at even lower frequencies and wider bandwidth without the need for additional dimensions.

Keywords—antenna; bandwidth enhancement; broadband frequency; circular-shaped; modified ground

I. INTRODUCTION

ANTENNA serve as crucial components in wireless communication systems, garnering significant attention in extensive research. In recent years, numerous wireless communication technologies have emerged, including wireless local area networks (WLANs), ultra-wideband communication (UWB), and cellular-based communications like 3G, 4G, and 5G networks. UWB and 4G/5G technologies have become focal points in the antenna field due to their status as the latest technologies [1]–[3]. This is attributed to their exceptionally broad bandwidth, enabling data transmission rates ranging from hundreds of megabytes to gigabytes, making them highly promising for diverse communication systems. In detail, UWB and 4G/5G technologies represent appealing and prospective solutions that bolster modern communication systems with

various benefits, encompassing capacity, speed, and performance across numerous wireless applications [4]–[6].

These technologies operate across multiple frequency bands, necessitating antennas with wideband capabilities. However, designing microstrip antennas with wide bandwidth and low-frequency capabilities presents several challenges. These difficulties primarily arise due to the relatively small size of the microstrip in comparison to the operating frequency. Therefore, achieving a combination of enhanced bandwidth and lower-frequency cut-off becomes crucial to support a broad frequency range of communication technologies. [1]–[3], [7], [8]

There are several interesting methods to enhance the antenna bandwidth, such as stacked structure [9], FIFA-structure [10], fourleaf clover [11], multiple parasitic patches [12], coplanar waveguide fed ring slot [13], metamaterial single rectangular split ring resonator [14], fractal-ground loaded frequency-reconfigurable [15]. Moreover, Chao Sun et al propose bandwidth truncation in a loaded patch antenna using the transmission line (TL) method model [16]. The study explores the combination of the truncated structure with proposed bandwidth enhancement characteristics, along with the integration of a compact circularly polarized patch antenna featuring the proposed complementary split ring structure. Two noteworthy conclusions are drawn from the study. Firstly, the results derived from the TL method model offer valuable insights and guidelines for patch antenna design. Secondly, the proposed structure proves to be an optimal replacement for conventional strip shorting techniques due to its inherent compactness and wideband attributes. Consequently, the proposed antenna design stands as an excellent alternative choice for compact circular patch antennas with amplified bandwidth requirements. However a bandwidth is still narrow.

Moreover, Wen-Ling Chen et al propose experimental exploration of a pioneering wide slot antenna proposal, synergistically integrating a microstrip line with a fractal-shaped slot to unlock remarkable improvements in bandwidth

*This work is supported by the Kementerian Pendidikan, Kebudayaan, Riset, dan Teknologi of Indonesia. Universitas Sultan Ageng Tirtayasa. 2023.

Siswo Wardoyo, Jaka Permana, and Teguh Firmansyah, are with Department of Electrical Engineering, Universitas Sultan Ageng Tirtayasa, Jl. Jenderal Sudirman Km 3, Cilegon, Indonesia (e-mails: Corresponding author siswo@untirta.ac.id; jakaper@gmail.com; teguhfirmansyah@untirta.ac.id).

Toto Supriyanto is with the Department of Telecommunication Engineering, Jl. G.A. Siwabessy, Depok, Indonesia (e-mail: tosupr@yahoo.com).

Muh Wildan is with the Politeknik Penerbangan Indonesia. Jl. Raya PLP Curug, Tangerang, Indonesia (e-mail: muh.wildan@ppicurug.ac.id).

Febrizal is with the Department of Electrical Engineering, Universitas Riau. Jl. Soebrantas Km. 12.5, Indonesia (e-mail: febrizal@eng.unri.ac.id).

Syah Alam is with the Department of Electrical Engineering, Universitas Trisakti, Jakarta, Indonesia (e-mail: syah.alam@trisakti.ac.id).



performance [17]. The strategic incorporation of the fractal-shaped slot unveils in operational bandwidth. The study delves into the intricate relationship between bandwidth and the iteration order (IO) and iteration factor (IF) of the fractal shape, employing a series of designed experiments. The experimental results affirm the proposed fractal slot antenna, as evidenced by its impressive impedance bandwidth. With a 10 dB reflection coefficient, this antenna achieves a 2.4 GHz operational bandwidth, strategically poised at approximately 4 GHz. Notably, the antenna has a minimum 2-dB gain bandwidth of 1.59 GHz.

The antenna with asymmetric rectangular patch featuring a U-shaped open slot structure, resulting in the realization of multiple resonances is proposed by [18]. Furthermore, the integration of two precision-engineered bevels on the patch serves to further optimize impedance matching. Through comprehensive experimental evaluations, the antenna exhibits an impressive 122% impedance bandwidth, spanning from 2.95 to 12.1 GHz, accompanied by a remarkable 10 dB return loss. Notably, this design achieves a substantial enhancement in impedance bandwidth, catapulting from a 28% to an 122% across an array of antenna configurations. However, the antenna structure is complex and the bandwidth is low.

As a novelty, this paper introduces a method to enhance the bandwidth of a circular microstrip antenna using an inverted C-shaped ground configuration, as depicted in Figure 1. Specifically, Figure 1(a), 1(b), and 1(c) illustrate a conventional circular microstrip antenna [Antenna 1], a circular microstrip antenna with a rotated C-shaped ground configuration [Antenna 2], and a circular microstrip antenna with an inverted C-shaped ground configuration [Antenna 2], respectively. The proposed method successfully extends the antenna's bandwidth while reducing the operating frequency. The antenna was simulated and fabricated using an RO5880 duroid substrate with a relative permittivity of 2.2, a thickness of 1.575 mm, and a loss tangent of 0.0009.

Moreover, this paper is organized as follows: Section II describes the antenna design and dimensions, Section III explains the antenna optimization process, Section IV describes the simulations and measurements, and finally, it concludes with a summary in the concluding section.

II. ANTENNA DESIGN

The main shape antenna patch radiator is circular. Then, the radius (g) of circular-shaped microstrip patch antenna is formulated by [19]–[21];

$$g = \frac{A}{\sqrt{1 + \frac{2h}{\pi\epsilon_r} \left[\ln \left(\frac{\pi P}{2h} \right) + 1.7726 \right]}} \quad (1)$$

where

$$P = \frac{8.791 \times 10^9}{f_r \sqrt{\epsilon_r}} \quad (2)$$

Moreover, this research paper utilizes the direct feeding method with a substrate of thickness (h) in centimeters and permittivity (ϵ_r). The resonant frequency (f_r) is important. The substrate's impedance (Z_0) is determined by the W/h ratio,

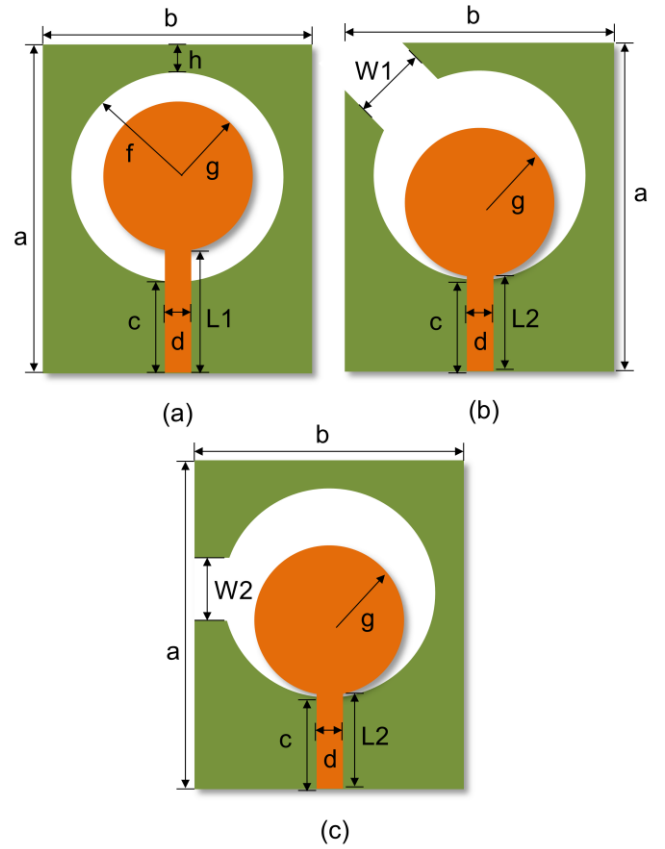


Fig. 1. (a) Conventional circular structure microstrip antenna [Antenna 1], (b) circular structure microstrip antenna based on rotated C-shaped ground configuration [Antenna 2], (c) circular structure microstrip antenna based on inverted C-shaped ground configuration [Antenna 2],

referenced from [19]–[21]. When $Z_0 \sqrt{\epsilon_r} > 89.91$, the appropriate W/h ratio can be determined by [19]–[21];

$$W/h = \frac{8 \exp(A)}{\exp(2A) - 2} \quad (3)$$

When $Z_0 \sqrt{\epsilon_r} \leq 89.91$, W/h ratio is given by [19]–[21];

$$W/h = \frac{2}{\pi} \left\{ B - 1 - \ln(2B - 1) + \frac{\epsilon_r - 1}{2\epsilon_r} \left[\ln(B - 1) + 0.39 - \frac{0.61}{\epsilon_r} \right] \right\} \quad (4)$$

where

$$A = \frac{Z_0}{60} \left\{ \frac{\epsilon_r + 1}{2} \right\}^{1/2} + \frac{\epsilon_r - 1}{\epsilon_r + 1} \left\{ 0.23 + \frac{0.11}{\epsilon_r} \right\} \quad (5)$$

$$B = \frac{60\pi^2}{Z_0 \sqrt{\epsilon_r}} \quad (6)$$

$$\epsilon_{re} = \frac{\epsilon_r + 1}{2} + \frac{\epsilon_r - 1}{2} F \left(\frac{W}{h} \right) \quad (7)$$

In general, Figure 1(a) illustrates a conventional circular microstrip antenna [Antenna 1]. The antenna has a circular patch with direct feeding. Meanwhile, the ground plane has a circular slot with its center coinciding with the center of the patch. The radius of the circular slot in the ground plane is larger than the radius of the patch.

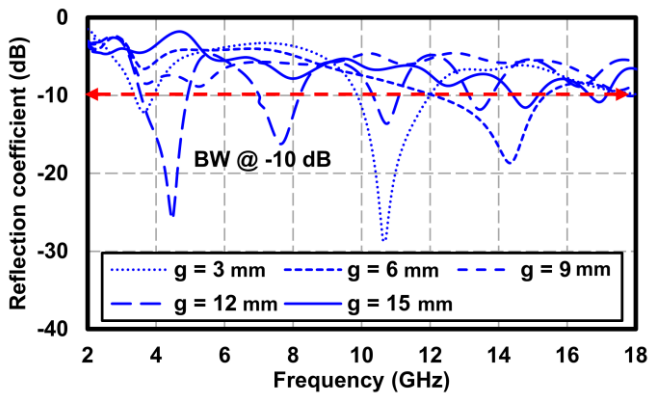


Fig. 2. The variation of antenna radius (g) from 5 to 15 and its impact on the reflection coefficient.

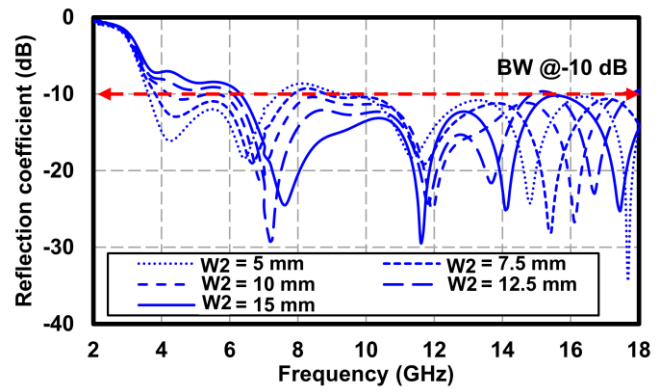


Fig. 4. The variation of dimension of (W_2) and its effect on reflection coefficient values from 2 – 18 GHz.

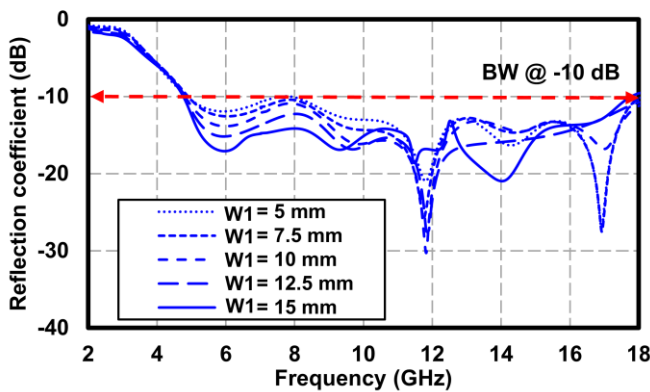


Fig. 3. The variation of dimension of (W_1) and its effect on reflection coefficient values from 2 – 18 GHz.

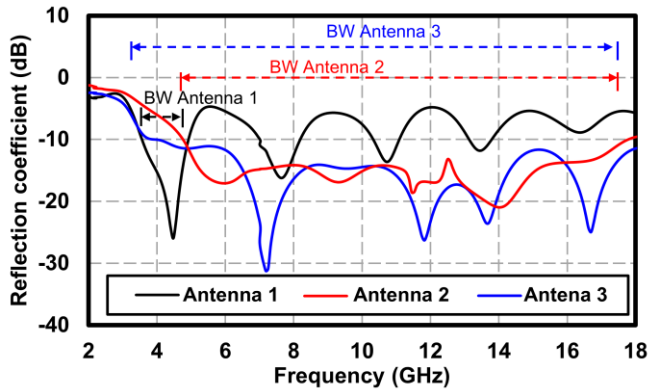


Fig. 5. Comparison results of antenna 1, antenna 2, and antenna 3.

Figure 1(b) illustrates a circular structure microstrip antenna based on a rotated C-shaped ground configuration [Antenna 2]. On the patch or radiator side, this antenna has the same radius as [Antenna 1]. However, it has a different feeding length. Additionally, this antenna has a circular slot on the ground side with an added slit on the corner, with a width of W_1 . The overall dimensions are the same as [Antenna 1].

Meanwhile, Figure 1(c) shows an antenna with a circular structure microstrip antenna based on an inverted C-shaped ground configuration [Antenna 3]. The structure of the radiator of this antenna is the same as Antenna 2. However, on the ground side, it has a slit pointing sideways, forming an inverted letter C. The total dimensions of antennas 1, 2, and 3 are identical. Meanwhile, the respective dimensions of each side are $a = 45$ mm, $b = 40$ mm, $c = 10.4$ mm, $d = 2.6$ mm, $f = 15$ mm, $g = 10$ mm, and $h = 3$ mm.

III. ANTENNA OPTIMIZATION

Figure 2 illustrates the variation of antenna radius (g) from 5 to 15 and its impact on the reflection coefficient. It is evident that the radius plays a crucial role in determining the antenna's operating frequency. At $g = 3$ mm, the antenna resonates at a frequency of 11.2 GHz with a reflection coefficient of -27.3 dB. Meanwhile, at $g = 6$ mm, the antenna exhibits reduced resonance with the lowest reflection value occurring at 14.2 GHz with -18 dB. On the other hand, for $g = 12$ mm, the antenna tends to resonate at 4.5 GHz with multiband characteristics. Ultimately, in order to achieve a wide bandwidth, a broad

response is required, which involves seeking non-dominant values. For this study, a radius of 10 mm was selected.

Figure 3 illustrates the variation of dimension (W_1) and its impact on reflection coefficient values from 2 to 18 GHz. Reducing the length of the feedline and adding a slot, W_1 , on the ground side can result in a wideband response. At $W_1 = 5$ mm, the lower cutoff frequency is 5 GHz with a slight increase in the reflection coefficient value at 8 GHz, exceeding -10 dB. Meanwhile, the best performance is achieved when W_1 is equal to 15 mm. However, for all W_1 values, the lower cutoff frequency remains at 5 GHz. Therefore, further steps are needed to decrease the lower cutoff frequency.

Figure 4 shows the variation of dimension (W_2) and its impact on reflection coefficient values from 2 to 18 GHz. The figure demonstrates that reducing the length of the feeding and adding a slot, W_2 , can significantly enhance the bandwidth. At $W_2 = 15$ mm, the lower cutoff frequency is 6.3 GHz with a reflection coefficient value of -23.3 dB. Conversely, at $W_2 = 5$ mm, the lower cutoff frequency is 3.8 GHz with a reflection coefficient value of -18.4 dB. However, there is a suboptimal reflection coefficient value around 8.1 GHz, exceeding -10 dB. The best performance is achieved at $W_2 = 10$ mm, where the lower cutoff frequency is 3.3 GHz, and the reflection coefficient value is <-10 dB at all locations.

Figure 5 shows a comparison results of antenna 1, antenna 2, and antenna 3. This comparison demonstrates that antenna 1 exhibits a multiband frequency response bandwidth. On the other hand, antenna 2 provides a wide bandwidth, but it has a

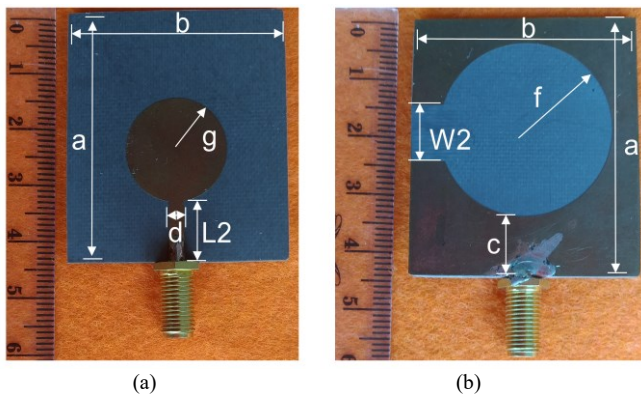


Fig. 6. Photograph of fabrication antenna 3. (a) patch plane with circular shaped, (b) ground-plane with inverted C-shaped structure.

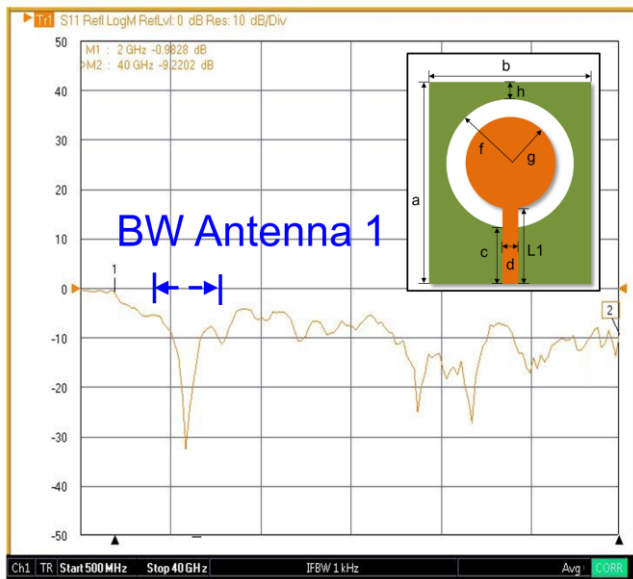


Fig. 7. Measurement result of reflection coefficient of antenna 1.

lower cutoff frequency at 5 GHz. The optimal result is obtained by antenna 3, which offers a wide bandwidth with a low cutoff frequency. This is advantageous as it supports the handling of wideband technologies.

IV. RESULT AND DISCUSSION

Figure 6(a) and 6(b) show photograph of fabrication antenna 3 patch of plane with circular shaped and ground-plane with inverted C-shaped structure, respectively. The antenna was fabricated using an RO5880 duroid substrate with a relative permittivity of 2.2, a thickness of 1.575 mm, and a loss tangent of 0.0009.

Figure 7 shows the measurement results of the reflection coefficient for antenna 1. The measurements indicate that the antenna operates at a lower frequency of approximately 3.7 GHz with a reflection coefficient value of -31.2 dB. Meanwhile, the bandwidth achieved is around 3.30 GHz. Additionally, the measurements also reveal that the antenna operates at a frequency of 10.1 GHz. However, it is observed that the antenna has values of the reflection coefficient greater than -10 dB at other frequencies. This limits the antenna's ability to operate in the ultra-wideband range.

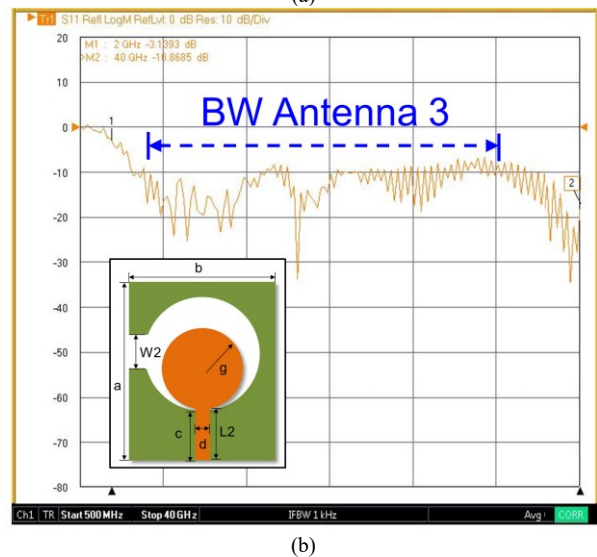
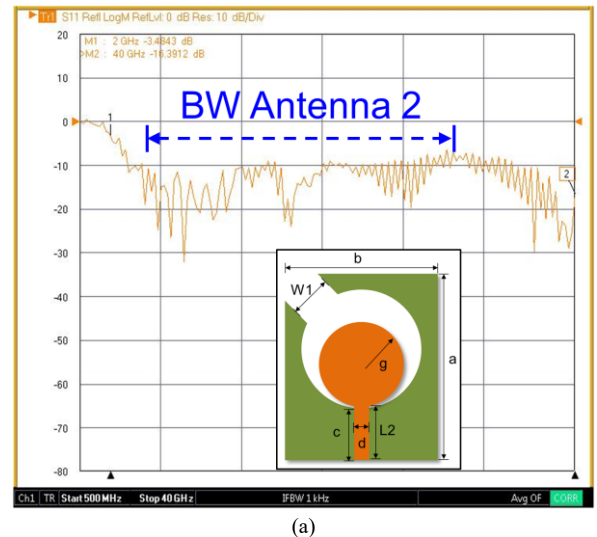


Fig. 8. Measurement result of reflection coefficient of (a) antenna 2, and (b) antenna 3.

Figure 8(a) presents the measurement results of the reflection coefficient for antenna 2. This antenna has a lower cutoff frequency of 3.70 GHz and a bandwidth of approximately 12.30 GHz. The minimum reflection coefficient value is below -30 dB. There are some ripples observed in the reflection coefficient values at the frequency of 6 GHz. However, the coefficient value at that frequency remains below -10 dB, which still falls within the antenna's bandwidth.

Continuing, Figure 8(b) illustrates the measurement results of the reflection coefficient for antenna 3. The measurements show that the antenna operates at a frequency of 3.30 GHz with a bandwidth of approximately 14.70 GHz. The best reflection coefficient value achieved is -33.1 dB. Some ripples are observed at 11.2 GHz, but they remain within the limit of <-10 dB, which still falls within the antenna's bandwidth. However, the reflection coefficient value goes above -10 dB at a frequency of 18 GHz. Consequently, the antenna operates, in general, in the frequency range from 3.3 GHz to 18 GHz.

Figure 9 (a)-(e) presents the surface current distribution at frequencies of 3.3 GHz, 3.5 GHz, 5.8 GHz, 10 GHz, and 18 GHz, respectively. It is evident that the highest current at 3.3 GHz occurs at Ia1 and Ia2. A clearer visualization of the

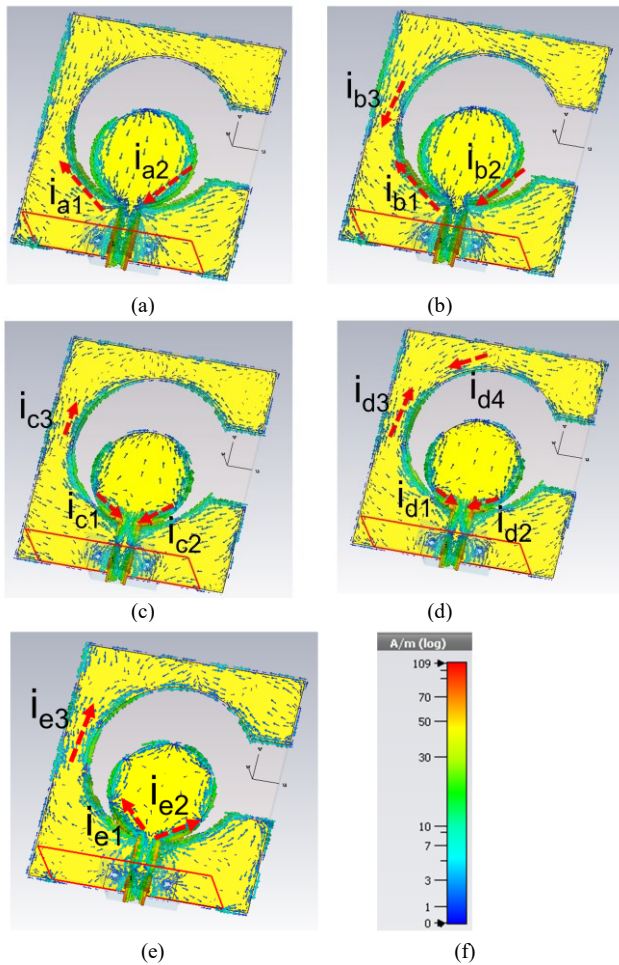


Fig. 9. Surface current distribution at frequency of (a) 3.3 GHz, (b) 3.5 GHz, (c) 5.8 GHz, (d) 10 GHz, and (e) 18 GHz.

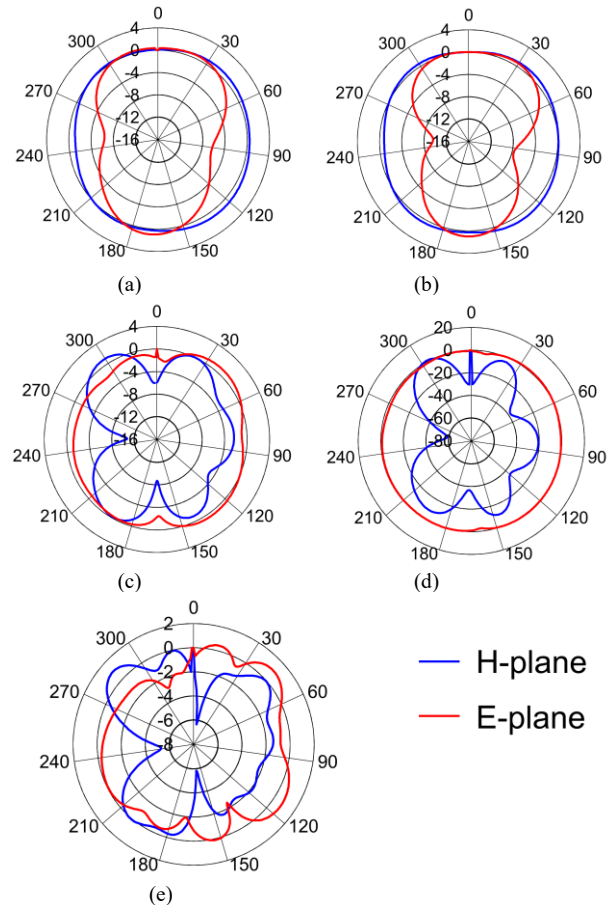


Fig. 10. Radiation pattern at frequency of (a) 3.3 GHz, (b) 3.5 GHz, (c) 5.8 GHz, (d) 10 GHz, and (e) 18 GHz.

maximum current and its direction can be observed in Figure 9. Notably, each frequency exhibits a different location and direction for its maximum current. The maximum current scale of 10 A/m was utilized.

Furthermore, Figure 10 illustrates the radiation pattern at frequencies of 3.3 GHz, 3.5 GHz, 5.8 GHz, 10 GHz, and 18 GHz. Overall, the proposed antenna demonstrates an omnidirectional pattern. Table 1 provides a comparison between the proposed antenna and previous designs. Overall, this research has successfully designed an antenna capable of operating in the ultra-wideband range, starting from a frequency of 3.3 GHz with a bandwidth of up to 14.7 GHz. These results demonstrate that the antenna's bandwidth can be increased from both the lower and upper cut-off frequency perspectives without the need to add antenna dimensions.

V. CONCLUSION

This paper presents a method for enhancing the bandwidth of a circular microstrip antenna based on an inverted C-shaped ground configuration. The proposed method successfully creates an antenna with extended bandwidth while lowering the frequency. The antenna was simulated and then fabricated using - an RO5880 duroid substrate with a relative permittivity of 2.2, a thickness of 1.575 mm, and a loss tangent of 0.0009. The total dimension of antenna is 40 mm x 45 mm. Then, the simulation

TABLE I
COMPARISON RESULT WITH PREVIOUS RESEARCH

Ref.	Method	Size (mm)	Low freq cut-off (GHz)	Bandwidth (GHz)
[14]	Metamaterial single rectangular split ring resonator	20.0 x 18.0	5.46	1.24
[21]	DGS based monopole circular-shaped patch	40.0 x 20.0	2.50	8.10
[15]	Metamaterial fractal ground loaded	51.9 x 51.9	1.40	8.12
[16]	Coupled Shorting Strip	35.0 x 35.0	1.25	0.20
[17]	Microstrip-line-fed with a fractal-shaped slot	70.0 x 70.0	3.30	2.10
[18]	Asymmetrical patch with U-shaped open-slot	24.5 x 24.5	2.95	9.15
This work	O-shaped ground plane [Antenna 1]	45 x 40	3.70	3.30
	Rotated C-shaped ground plane [Antenna 2]	45 x 40	3.70	12.30
	Inverted C-shaped ground plane [Antenna 3]	45 x 40	3.30	14.70

and measurement results demonstrate that the antenna can operate effectively within a wide frequency range of 3.3 GHz to 18 GHz with bandwidth 14.7 GHz. Additionally, utilizing this method enables the antenna to function at even lower frequencies without the need for additional dimensions.

REFERENCES

- [1] W. Hong *et al.*, "Multibeam antenna technologies for 5g wireless communications," *IEEE Trans. Antennas Propag.*, vol. 65, no. 12, pp. 6231–6249, 2017, <http://doi.org/10.1109/TAP.2017.2712819>
- [2] T. Li and Z. N. Chen, "Shared-surface dual-band antenna for 5g applications," *IEEE Trans. Antennas Propag.*, vol. 68, no. 2, pp. 1128–1133, 2019, <http://doi.org/10.1109/TAP.2019.2938584>.
- [3] W. Hong, K.-H. Baek, and S. Ko, "Millimeter-wave 5g antennas for smartphones: overview and experimental demonstration," *IEEE Trans. Antennas Propag.*, vol. 65, no. 12, pp. 6250–6261, 2017, <http://doi.org/10.1109/TAP.2017.2740963>.
- [4] K. S. Radhakrishna, M. S. Shakhirul, Y. S. Lee, K. N. Khairina, and A. R. A. Syafiqah, "Investigate bending effect of wearable gps patch antenna with denim and polyester fabric substrate," *Int. J. Electron. Telecommun.*, vol. 69, no. 2, pp. 225–231, 2023, <http://doi.org/10.24425/ijet.2023.144354>.
- [5] S. H. Hussein and K. K. Mohammed, "A dual-band compact integrated rectenna for implantable medical devices," *Int. J. Electron. Telecommun.*, vol. 69, no. 2, pp. 239–245, 2023, <http://doi.org/10.24425/ijet.2023.144356>.
- [6] A. Ghodake and B. Hogade, "Wearable textile antenna for glucose level monitoring," *Int. J. Electron. Telecommun.*, vol. 69, no. 2, pp. 219–224, 2023, <http://doi.org/10.24425/ijet.2023.144353>.
- [7] D. Liu, W. Hong, T. S. Rappaport, C. Luxey, and W. Hong, "What will 5g antennas and propagation be?," *IEEE Trans. Antennas Propag.*, vol. 65, no. 12, pp. 6205–6212, 2017, <http://doi.org/10.1109/TAP.2017.2774707>.
- [8] I. Ahmad, W. Tan, Q. Ali, and H. Sun, "Latest performance improvement strategies and techniques used in 5g antenna designing technology, a comprehensive study," *Micromachines*, vol. 13, no. 5, p. 717, 2022, <http://doi.org/10.3390/mi13050717>.
- [9] J. Shi, X. Geng, S. Yan, K. Xu, and Y. Chen, "An approach to achieving multiple mutual coupling nulls in mimo stacked patch antenna for decoupling bandwidth enhancement," *IEEE Trans. Circuits Syst. II Express Briefs*, vol. 69, no. 12, pp. 4809–4813, 2022, <http://doi.org/10.1109/TCSII.2022.3196020>.
- [10] C. Lee, T. Yo, F. Huang, and C. Luo, "Bandwidth enhancement of planar inverted-f antenna for implantable biotelemetry," *Microw. Opt. Technol. Lett.*, vol. 51, no. 3, pp. 749–752, 2009, <http://doi.org/10.1002/mop.24189>.
- [11] Y. Cui, L. Wu, and R. Li, "Bandwidth enhancement of a broadband dual-polarized antenna for 2g/3g/4g and imt base stations," *IEEE Trans. Antennas Propag.*, vol. 66, no. 12, pp. 7368–7373, 2018, <http://doi.org/10.1109/TAP.2018.2867046>.
- [12] K. Da Xu, H. Xu, Y. Liu, J. Li, and Q. H. Liu, "Microstrip patch antennas with multiple parasitic patches and shorting vias for bandwidth enhancement," *IEEE Access*, vol. 6, pp. 11624–11633, 2018, <http://doi.org/10.1109/ACCESS.2018.2794962>.
- [13] K. Saraswat and A. R. Harish, "Analysis of wideband circularly polarized ring slot antenna using characteristics mode for bandwidth enhancement," *Int. J. RF Microw. Comput. Eng.*, vol. 28, no. 2, p. e21186, 2018, <http://doi.org/10.1002/mmce.21186>.
- [14] T. Ali, M. S. Aw, and R. C. Biradar, "AA compact bandwidth enhanced antenna loaded with srr for wlan/wimax/satellite applications," *Adv. Electromagn.*, vol. 7, no. 4, pp. 78–84, 2018, <http://doi.org/10.7716/aem.v7i4.644>.
- [15] S. Das, A. Gupta, and S. Sahu, "Metamaterial based fractal-ground loaded frequency-reconfigurable monopole-antenna with gain-bandwidth enhancement," *AEU-International J. Electron. Commun.*, vol. 132, p. 153593, 2021, <http://doi.org/10.1016/j.aeue.2020.153593>.
- [16] C. Sun, H. Zheng, L. Zhang, and Y. Liu, "Analysis and design of a novel coupled shorting strip for compact patch antenna with bandwidth enhancement," *IEEE Antennas Wirel. Propag. Lett.*, vol. 13, pp. 1477–1481, 2014, <http://doi.org/10.1109/LAWP.2014.2341596>.
- [17] W. Chen, G. Wang, and C. Zhang, "Bandwidth enhancement of a microstrip-line-fed printed wide-slot antenna with a fractal-shaped slot," vol. 57, no. 7, pp. 2176–2179, 2009, <http://doi.org/10.1109/TAP.2009.2021974>.
- [18] W. X. Liu, Y. Z. Yin, W. L. Xu, and S. L. Zuo, "Compact open-slot antenna with bandwidth enhancement," *IEEE Antennas Wirel. Propag. Lett.*, vol. 10, pp. 850–853, 2011, <http://doi.org/10.1109/LAWP.2011.2165197>.
- [19] A. Dastranj, F. Ranjbar, and M. Bornapour, "A new compact circular shape fractal antenna for broadband wireless communication applications," *Prog. Electromagn. Res. C*, vol. 93, pp. 19–28, 2019, <http://doi.org/10.2528/PIERC19031001>.
- [20] T. Addepalli and V. R. Anitha, "A very compact and closely spaced circular shaped uwb mimo antenna with improved isolation," *AEU-International J. Electron. Commun.*, vol. 114, p. 153016, 2020, <http://doi.org/10.2528/PIERC19031001>.
- [21] D. Gopi, A. R. Vadaboyina, and J. R. K. K. Dabbakuti, "DGS based monopole circular-shaped patch antenna for uwb applications," *SN Appl. Sci.*, vol. 3, no. 2, p. 198, 2021, <http://doi.org/10.1007/s42452-020-04123-w>.